Progress in Additive Manufacturing
https://doi.org/10.1007/s40964-024-00573-5

FULL RESEARCH ARTICLE

A mathematical surface roughness model for objects made by material jetting

Pushkar Kamble[1] · Yash Mittal[1] · Gopal Gote[1] · Mayur Patil[1] · K. P. Karunakaran[1]

Received: 19 June 2023 / Accepted: 20 January 2024

Abstract
This study aims to develop a mathematical model of the surface roughness of objects produced by multi-jet printing at sub-zero temperatures. Previous research on Sub-zero Additive Manufacturing (SAM) has described the "Ice line Model" for single jet dispensing, which accounts for individual droplet geometry but ignores the staircase effect, which is a key cause of roughness in 3D printed products. The "Spherical Cap Model" for Stratasys' PolyJet process considers the staircase effect but does not consider individual droplet shape. The model presented in this paper addresses individual droplets in the same way as the ice line model, and the staircase effect in the same way as the spherical cap model, thus eliminating the drawbacks of both. Droplets per inch (DPI) and surface inclination are the two main criteria that influence surface roughness. Therefore, the sample objects were printed using a PolyJet-like custom-made Sub-zero Additive Manufacturing (SAM) machine with two DPI settings, 360 and 720, and ten different surface inclinations (0°, 10°, 20°, 30°, 40°,50°, 60°, 70°, 80°, 90°). The surface roughness of the sample parts was measured and compared to theoretical values calculated using a mathematical model. The proposed mathematical model is consistent with the experimental results and is found to predict the surface roughness values more accurately than previously existing models. A complete surface roughness model is presented in this paper for the multi-jet-based AM processes.

Keywords Mathematical model · Surface roughness model · 3D printing · Sub-zero temperature

1 Introduction

The present article investigates the surface roughness of the objects printed on an indigenously developed multi-jet based sub-zero temperature 3D printer. It has an inkjet printhead similar to PolyJet and MultiJet Printing (MJP) techniques. The novelty of the present research is that the authors use water and aqueous solutions as AM materials, which is unique. Very few studies are available that discuss the surface roughness of ice objects.

One of the earliest works reported for ice 3D printing is Rapid Freeze Prototyping (RFP) technique by M. C. Leu et al. RFP uses a piezoelectric nozzle that dispenses water in a layered fashion to realize the ice parts [1–6]. The surface roughness of the ice parts is modelled using *ice line* analysis which assumes that the nozzle is dispensing a single line of water layer-by-layer to create a wall [2, 6].

Several studies are available on the surface roughness of the polyjet parts which discuss the experimentally found surface roughness [7–14]. Krishnan and Gurunathan (2015) have elaborated on the theoretical and experimental surface roughness obtained by the PolyJet process [9]. They employ a model of individual droplets in the shape of *a spherical cap*. They have optimized the surface finish using three parameters: layer thickness, type of finish (glossy or matte), and local surface orientation. Experimentally observed surface roughness values for *the PolyJet* process are reported by Kechagias and Maropoulos (2015) [7]. There is another study of surface roughness available with indigenously developed multi-jet AM machine by Y. L. Cheng et al., but they use roller for levelling and obtain smoother surface, hence, it is not considered [15]. Ice line and spherical cap models are explained in detail subsequently.

✉ Pushkar Kamble
pushkarkamble@gmail.com

[1] Department of Mechanical Engineering, Indian Institute of Technology Bombay, Mumbai 400076, India

Published online: 07 March 2024

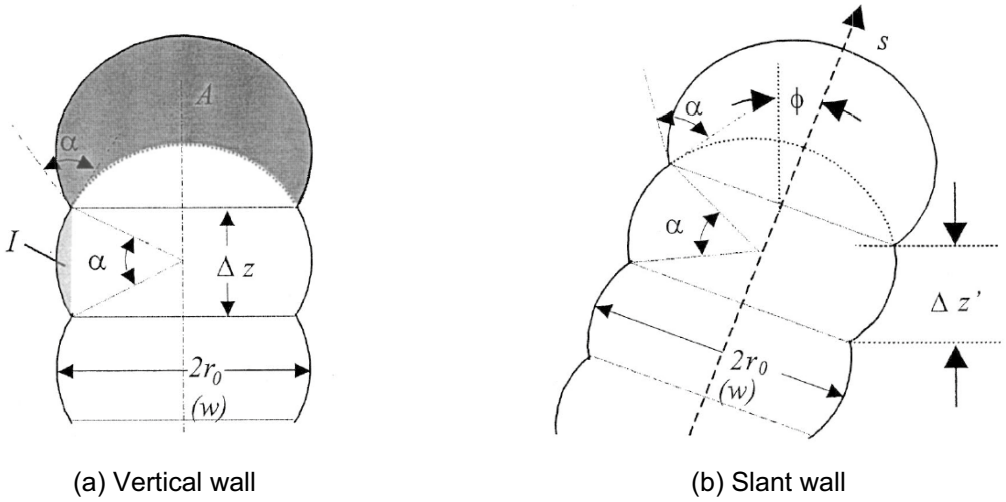

(a) Vertical wall (b) Slant wall

Fig. 1 Cross-section of ice line [2]

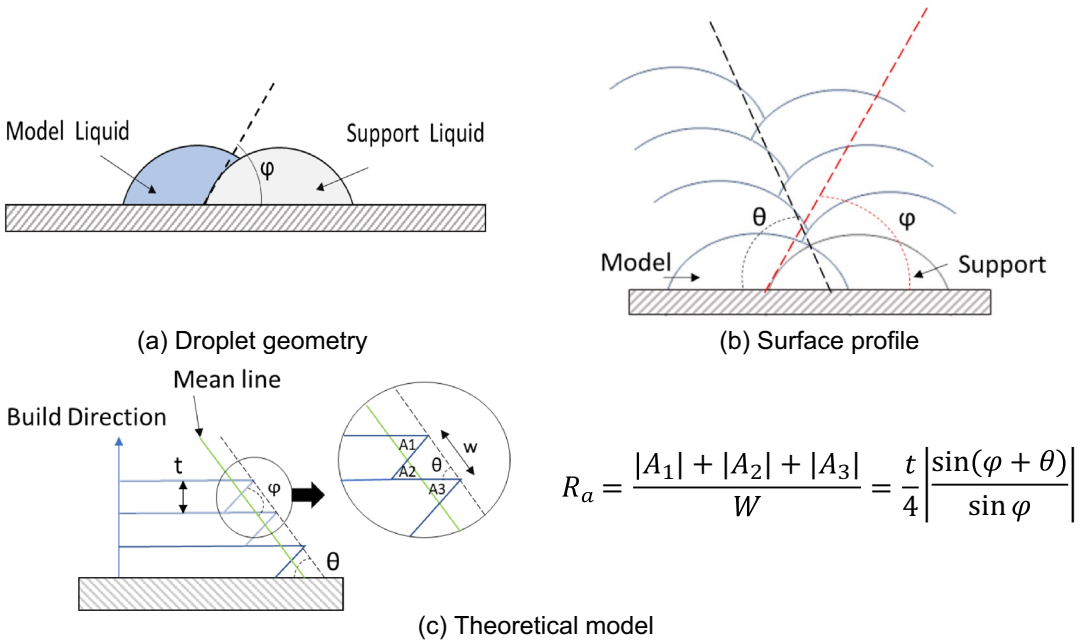

(a) Droplet geometry (b) Surface profile

$$R_a = \frac{|A_1| + |A_2| + |A_3|}{W} = \frac{t}{4}\left|\frac{\sin(\varphi + \theta)}{\sin\varphi}\right|$$

(c) Theoretical model

Fig. 2 Spherical cap model [9]

1.1 Ice line model

The ice line model is developed, assuming the droplets are deposited in a line. Multiple such passes stack the droplets in layers to form an ice line, as shown in Fig. 1. According to this model, surface irregularities are caused by droplets freezing and forming a spherical shape.

The sphericity of the forming droplets causes surface imperfections, as demonstrated in Fig. 1a, b. In the case of a slant surface, an angle ϕ is considered, the remaining parameters being the same for the ice line. This model considers the waviness of the surface due to the droplet sphericity. However, this model does not consider the staircase effect, a crucial cause of surface roughness in AM parts.

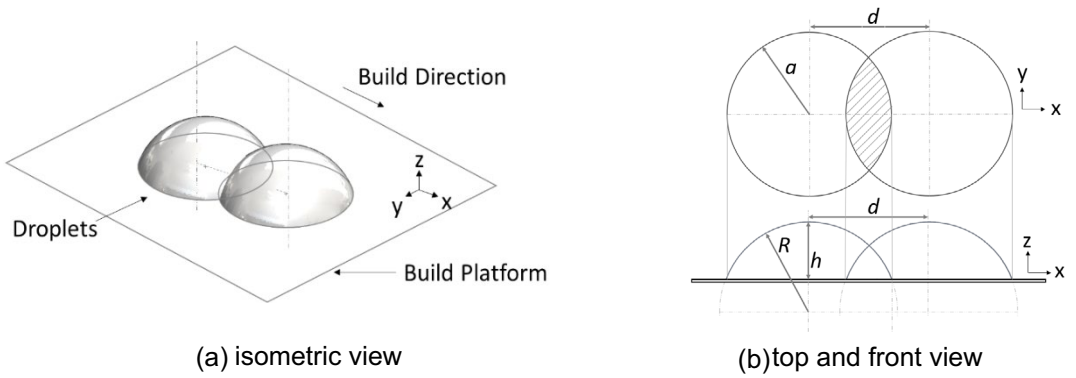

Fig. 3 Schematic representation of droplet formation: **a** isometric view, **b** top and front view

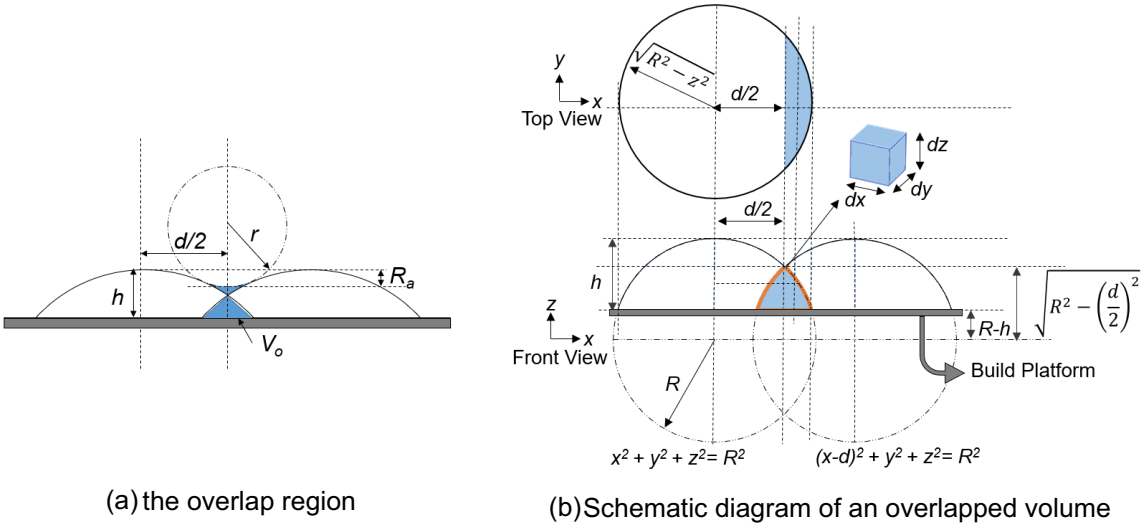

Fig. 4 Displaced volume between **a** the overlap region **b** Schematic diagram of an overlapped volume

1.2 Spherical cap model

The theoretical surface roughness achieved by the PolyJet technique has been explored by Kumar and Kumar [9]. They have optimized the surface finish with three parameters: layer thickness, type of finish (glossy or matte, which corresponds to the DPI; 360 and 720, respectively [9, 16]), and local surface orientation. As illustrated in Fig. 2, their model considers the *spherical cap* form of the droplets. Their material of interest is the resin generally used for the PolyJet technique.

The surface profile predicted by *the spherical cap model* is shown in Fig. 2a, b. Figure 2c gives the controlling parameters and mathematical representation of surface roughness (R_a), where φ is the contact angle of the droplet with the surface and θ is the inclination angle. The proposed model agrees well with the experimental results and is more suitable for the matte finish, i.e. lower DPI values in the PolyJet process. Kechagias and Maropoulos have experimentally verified the same, and have concluded that DPI, i.e. build style in terms of PolyJet (Glossy and Matte) affects the surface roughness the most [7]. The analysis is also fortified by the experimental analysis made by Kumar and Kumar.

As seen above, the *spherical cap model* considers the staircase effect; however, it does not consider the sphericity of the droplets, which is the source of the roughness in horizontal and inclined surfaces.

The authors propose a model that considers both individual droplet geometry and the staircase effect caused by slant surfaces. The proposed model overcomes these limitations in *ice line* and *spherical cap* models.

2 Proposed mathematical model

The proposed model assumes that the droplets take the shape of a spherical cap as soon as they land on the build platform, as illustrated in Fig. 3. The droplet that landed and

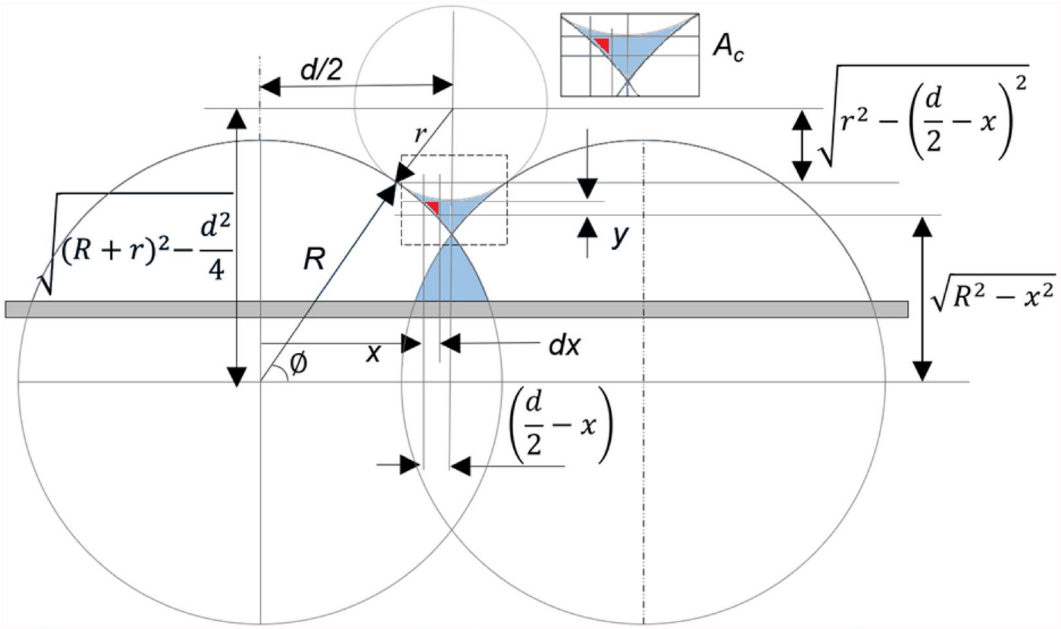

Fig. 5 Schematic diagram for estimation of overlap cross-sectional area

solidified on the surface is called a *bead* to distinguish it from the falling droplet. The surface tension and gravity of the bead determine its spread. Bond number (*Bo*), a dimensionless ratio of gravitational and capillary forces, indicates the spread [17].

$$Bo = \frac{\rho g d^2}{\sigma}, \tag{1}$$

where ρ is the density of the liquid in kg/m^3, g is the acceleration due to gravity, i.e. 9.81 m/s^2, d is the characteristic dimension. Generally, the radius of the curvature of the bead in m and σ is the surface tension in N/m. $Bo < 1$ indicates that surface tension is more influential, and $Bo > 1$ indicates gravity is more influential. In the present case for water, ρ is 1000 kg/m3, d is 1.23×10^{-5} m, and surface tension is 0.076 N/m. $Bo = 1.9 \times 10^{-5} \ll 1$. Therefore, the droplet spread is less and surface tension is more prominent, which gives the drop the shape of a spherical section, as shown in Fig. 3a. Because of the small volume of the droplets, it is assumed that they solidify as soon as they touch the built plate.

Layer thickness is found empirically. The object's height was measured after printing the known number of layers of an object to measure the layer thickness. Average layer height was calculated from the ratio of part height and the number of layers. The layer height was determined to be 6 µm.

2.1 Part A: Horizontal surface

Figure 3a depicts the beads. The dimensions of the bead are as illustrated in Fig. 3b:

h = layer thickness (height of the bead cross-section)
R = radius of the bead cross-section
a = radius of the bead at the build platform (overlapping circles in the top view)
d = centre distance between two consecutive beads
V_b = bead volume

Equation 2 can be used to calculate the radius of the bead at the build platform, a, for a known bead volume V_b and a predetermined layer height h. Equation 3 is used to compute the centre distance d between two consecutive drops as a function of *Droplets per Inch (DPI)*, a characteristic of the multi-jet dispensing process to determine deposition rate.

$$V_b = \frac{\pi h}{6}\left(3a^2 + h^2\right) \tag{2}$$

$$d = \frac{25.4 \times 10^3}{\mathrm{DPI} - 1}(\mu m) \tag{3}$$

The overlapped volume V_o is displaced towards the interface of the two beads in the form of curvature of radius r, as shown in Fig. 4a [18]. To determine V_o, a unit volume of dxdydz lying inside the overlap region between two beads is considered in Fig. 4a. X-axis limits are from $d/2$ to $\sqrt{R^2 - z^2 - y^2}$, as shown in Fig. 4b (Front View). Y limits range from 0 to $\sqrt{R^2 - z^2 - \left(\frac{d}{2}\right)^2}$, and Z limits range from $(R - h)$ to $\sqrt{R^2 - \left(\frac{d}{2}\right)^2}$.

As per the mentioned limits, the triple integral is formulated to determine the overlapped volume between the two droplets (Eq. 4).

$$V_o = 2\int_{R-h}^{\sqrt{R^2-(d/2)^2}}\int_{0}^{\sqrt{R^2-z^2-(d/2)^2}}\int_{d/2}^{\sqrt{R^2-z^2-y^2}} \mathrm{d}x\mathrm{d}y\mathrm{d}z$$

$$V_o = \frac{d}{4}\left[\left(R^2-\frac{d^2}{4}\right)\left(\frac{\pi}{2}-\sin^{-1}\left(\frac{R-h}{\sqrt{R^2-\frac{d^2}{4}}}\right)\right)-3(R-h)\sqrt{(2R-h)h-\frac{d^2}{4}}\right]$$

$$-(R-h)(2R-h)h\sin^{-1}\sqrt{1-\frac{d^2}{4(2R-h)h}} \tag{4}$$

As shown in Fig. 5, the displaced volume forms a meniscus with a radius r. A cross-sectional area A_c is considered to calculate r. It is symmetrical at about $x = d/2$. A small elemental area dxdz (marked red) is considered that lies within area A_c to determine Ac. A_c is symmetrical. ϕ is considered an angle subtended at the sphere centre at the contact point of the displaced water meniscus. It is determined within the limits of $R\cos\phi$ and $d/2$ in the X direction, as given in Eq. 5.

$$A_c = 2\int_{R\cos\emptyset}^{d/2} z\,\mathrm{d}x$$

$$= 2\int_{\frac{d}{2}\left(\frac{R}{r+R}\right)}^{d/2}\left(\sqrt{(R+r)^2-\frac{d^2}{4}}-\sqrt{r^2-\left(\frac{d}{2}-x\right)^2}-\sqrt{R^2-x^2}\right)\mathrm{d}x \tag{5}$$

$$= d\left(\frac{R}{r+R}\right)\sqrt{(R+r)^2-\frac{d^2}{4}}-r^2\left[\sin^{-1}\left(\frac{d}{2(R+r)}\right)+\frac{d}{2(R+r)}\sqrt{1-\left(\frac{\frac{d}{2}\left(\frac{R}{r+R}\right)}{R}\right)^2}\right]$$

$$-R^2\left[\sin^{-1}\left(\frac{d}{2R}\right)-\sin^{-1}\left(\frac{d}{2(R+r)}\right)+\frac{d}{2R}\sqrt{1-\frac{d^2}{4R^2}}-\frac{d}{2(R+r)}\sqrt{1-\frac{d^2}{4(R+r)^2}}\right]$$

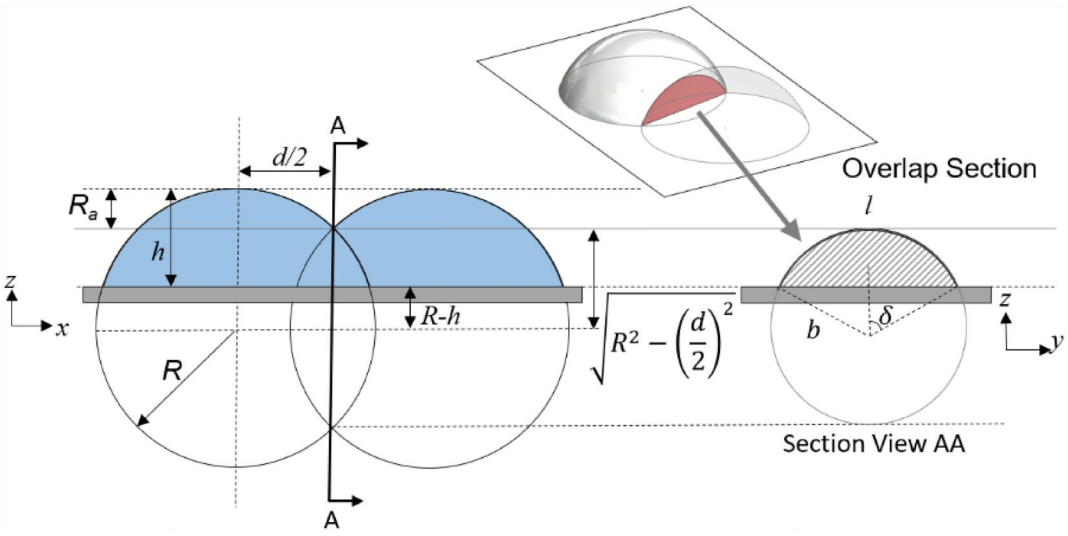

Fig. 6 Schematic for estimation of swept length

Table 1 Peak-to-valley surface roughness results

Sr. no	Property	Value
1	Bead Volume, V_b (μm^3)	5000
2	DPI	720
3	Layer height/spherical cap height, h (μm)	6
4	Radius of circumscribing sphere, R (μm)	48.3
5	Radius of the base circle, a (μm)	22.7
6	Droplet spacing, d (μm)	35.33
7	Overlapped volume, V_o (μm^3)	130.63
8	Contact length, l (μm)	31.05
9	Cross-sectional Area, A_c (μm^2)	4.21
10	Surface roughness, R_a (μm)	3.827

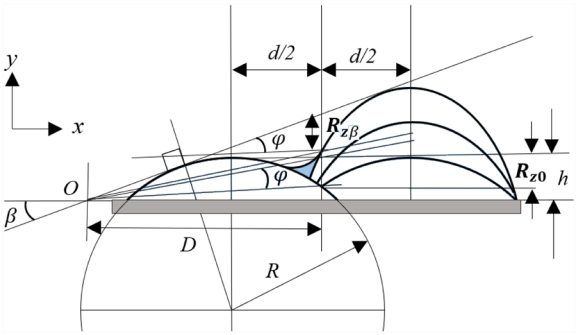

Fig. 7 Schematic for estimation of surface roughness on an inclined surface

Contact length l is the distance along the interface section of the two beads in the yz plane, as shown in Fig. 6. Mathematically, contact length is given by Eq. 6.

$$l = \frac{V_o}{A_c} \tag{6}$$

The contact length is also determined using Eq. 7.

$$l = 2\delta b = 2\left(\cos^{-1}\left(\frac{R-h}{\sqrt{R^2-\frac{d^2}{4}}}\right)\right)x\sqrt{R^2-\frac{d^2}{4}} \tag{7}$$

The values of V_o, A_c and l are substituted in Eq. 6 to determine r. For a given set of process parameters (droplet volume, layer height and DPI), the droplet dimensions and spacing (R, a, d) can be determined. These values are then used to calculate the overlapped volume and swept length. Further, the surface roughness is determined using Eq. 8.

$$R_a = h + r + \sqrt{R^2-a^2} - \sqrt{(R+r)^2-\frac{d^2}{4}}. \tag{8}$$

For a SAM system with a droplet volume as 5 pl (pico-litres) working at 720 DPI and 6 μm layer thickness, the surface roughness is 3.827 μm. Table 1 summarizes these results.

2.2 Part B: Inclined surface at an angle of β°

The above analysis is valid for a horizontal surface. The angle of inclination for the horizontal surface is 0°. Hence, roughness value is termed R_{a0}. For a surface inclined at an angle β, the roughness is termed $R_{a\beta}$. The fixed point (O) is marked at the intersection of the common tangents to the inclined surface and the horizontal axis, as shown in Fig. 7.

As the working scale is micro-level, it is assumed that the peak-to-valley distances for horizontal and inclined surface roughness lie on the same vertical axis. Figure 7 shows that the vertical axis is lying at the central distance between two consecutive drops of the first deposition layer. The distance between the vertical axis and the fixed point is denoted by D and is calculated using Eq. 9.

$$D = R\left[\frac{1-\left(1-\frac{h}{R}\right)\cos\beta}{\sin\beta}\right] + \frac{d}{2} \tag{9}$$

The angle subtended by the horizontal surface roughness at the fixed point is given by Eq. 10.

$$\varphi = \tan^{-1}\left(\frac{h}{D}\right) - \tan^{-1}\left(\frac{h-R_{z0}}{D}\right). \tag{10}$$

At the fixed point, the same angle is also subtended by the inclined surface roughness (Eq. 11).

$$\varphi = \beta - \tan^{-1}\left(\frac{D\tan\beta - R_{z\beta}}{D}\right). \tag{11}$$

By equating the angles from Eqs. 14 and 15 and solving for $R_{z\beta}$ yields the inclined surface roughness (Eq. 12).

$$R_{z\beta} = D\left[\tan\beta - \tan\left(\beta + \tan^{-1}\left(\frac{h-R_{z0}}{D}\right) - \tan^{-1}\left(\frac{h}{D}\right)\right)\right]. \tag{12}$$

Surface inclined at 90° is a particular case. It involves the deposition of the droplets precisely one above the other. Equation 12 does not help determine the R_a value since the tangent ratio is undefined at 90°. In order to determine the surface roughness over vertical, 90° inclination surfaces, the model proposed by Sui and Leu, 2003 is considered.

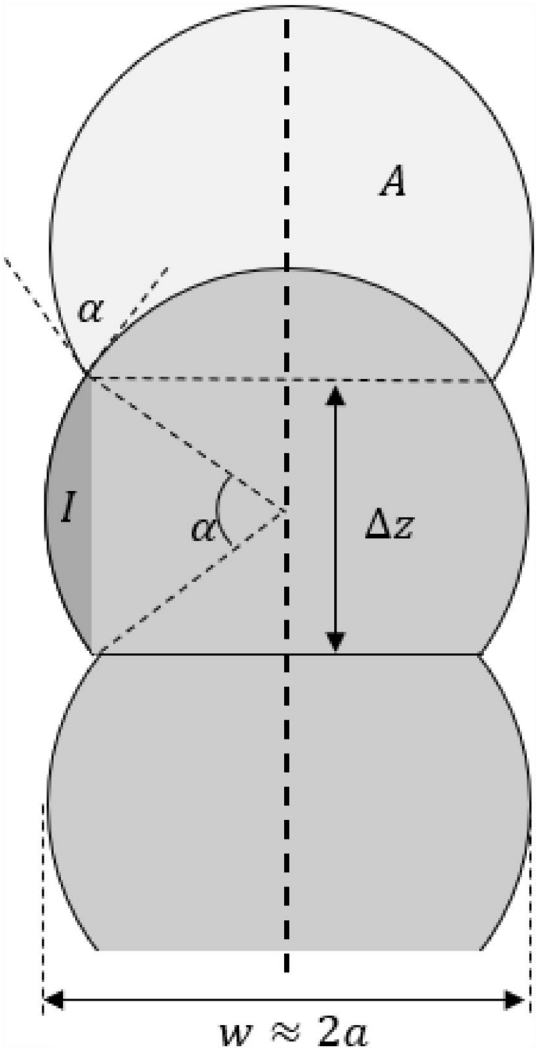

Fig. 8 Schematic for roughness estimation of vertical surface

According to their model, the surface roughness, R_a over a vertical surface is given by Eq. 13 [1],

$$R_a = \frac{I}{\Delta z} = \frac{\alpha - \sin\alpha}{8\sin^{3/2}(\alpha/2)}\sqrt{A}, \tag{13}$$

where I is the shaded area for the surface roughness calculation, Δz is the layer height, α is the water–ice contact angle, and A is the shaded area of the water line, as shown in Fig. 8.

The shaded area of the water line, A for a spherical cap (Fig. 8), is calculated using Eq. 14.

$$A = ah + R^2\left[\sin^{-1}\left(\frac{a}{R}\right) - \frac{a}{R}\right]. \tag{14}$$

Also, the water–ice contact angle, α, can be calculated by equating the layer height with line width, w (Eq. 15).

$$\Delta z = w\sin(\alpha/2). \tag{15}$$

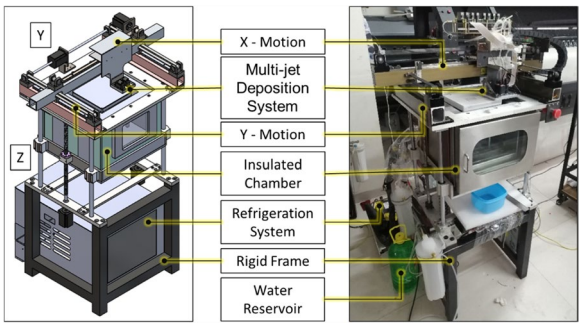

Fig. 9 Sub-zero additive manufacturing (SAM) machine

Solving for A & α, mean surface roughness, R_a for a vertical ice surface (90° inclination), with process parameters as mentioned in Table 1, came out to be 0.1 μm. It should be noted that the inter-droplet spacing should be less than the diameter of the base circle ($d < 2a$) for droplet overlap. For low values of DPI, such as 360, there is no overlap of the droplet. Hence, the peak-to-valley distance is the same as the layer height, h. For such cases, the horizontal surface roughness, R_a, is 6 μm. There is no droplet overlap at low DPI settings, such as 360. As a result, the peak-to-valley distance equals the layer height, h. In such circumstances, R_a was found to be 6 μm.

3 Experimental methods

Metals, ceramics, and polymers are the three broad categories of AM materials [19, 20]. However, AM technology is evolving, and some non-conventional materials such as water, aqueous solutions, gels, colloids and slurries are emerging as AM materials. These materials are liquid at room temperature. Hence, they require sub-zero temperatures for their deposition to create objects. Therefore, the technique is named Sub-zero Additive Manufacturing (SAM). M. C. Leu et al. [21], Pieter Sijpkes et al. [22], Zhang et al. [23], Zheng et al. [24], and Pushkar Kamble et al. [5, 25] have all demonstrated AM of ice objects.

With the advent of these materials, newer and environment-friendly applications are opening up for AM objects. One such application is using ice objects as patterns for investment casting. Traditionally, wax is used, which gives out hydrocarbons when melted for dewaxing the moulds. Ice is a much greener and cheaper alternative as compared to wax. Investment casting is well known for producing near-net-shape geometries with a smoother surface finish than sand casting. Hence, it is used for producing jewellery and dental implants. Therefore, it is essential to assess the surface roughness of the frozen objects produced by SAM.

Authors have developed a prototype of SAM based on the multi-jet dispensing technology similar to Stratasys' PolyJet (Fig. 9). It uses a multi-jet printer to distribute water and aqueous solution in the raster pattern layer by layer. The printhead has four rows of staggered nozzles, each row devoted to one liquid tank. There are 320 nozzles in each row of 28.8 mm. For model and support liquids, we deploy two rows each. The printhead driver software allows for selecting two DPIs, 360 and 720, which equate to dot sizes of 73 µm and 36 µm, respectively. The build process takes place inside a refrigerated chamber at −30 °C. The chamber size is 200 mm × 200 mm × 150 mm. The build platform and the chamber are maintained at −30 °C using a vapour compression refrigeration system augmented by liquid nitrogen for cooling.

The objective of the experiments is to determine the relationship between surface roughness and surface orientation at two distinct DPIs. Surface roughness is measured at five distinct orientations for 360 DPI and 720 DPI: 0°, 30°, 45°, 60°, and 90°. Surface orientation and DPI are two variables that can influence surface finish. A full factorial design was used for the experimental plan. Five values of the surface orientation angles (0°, 30°, 45°, 60° and 90°) and two values of the DPI (360, 720) lead to $5^1 \times 2^1 = 10$ experiments. These experiments were repeated four times to ensure that the results were statistically significant.

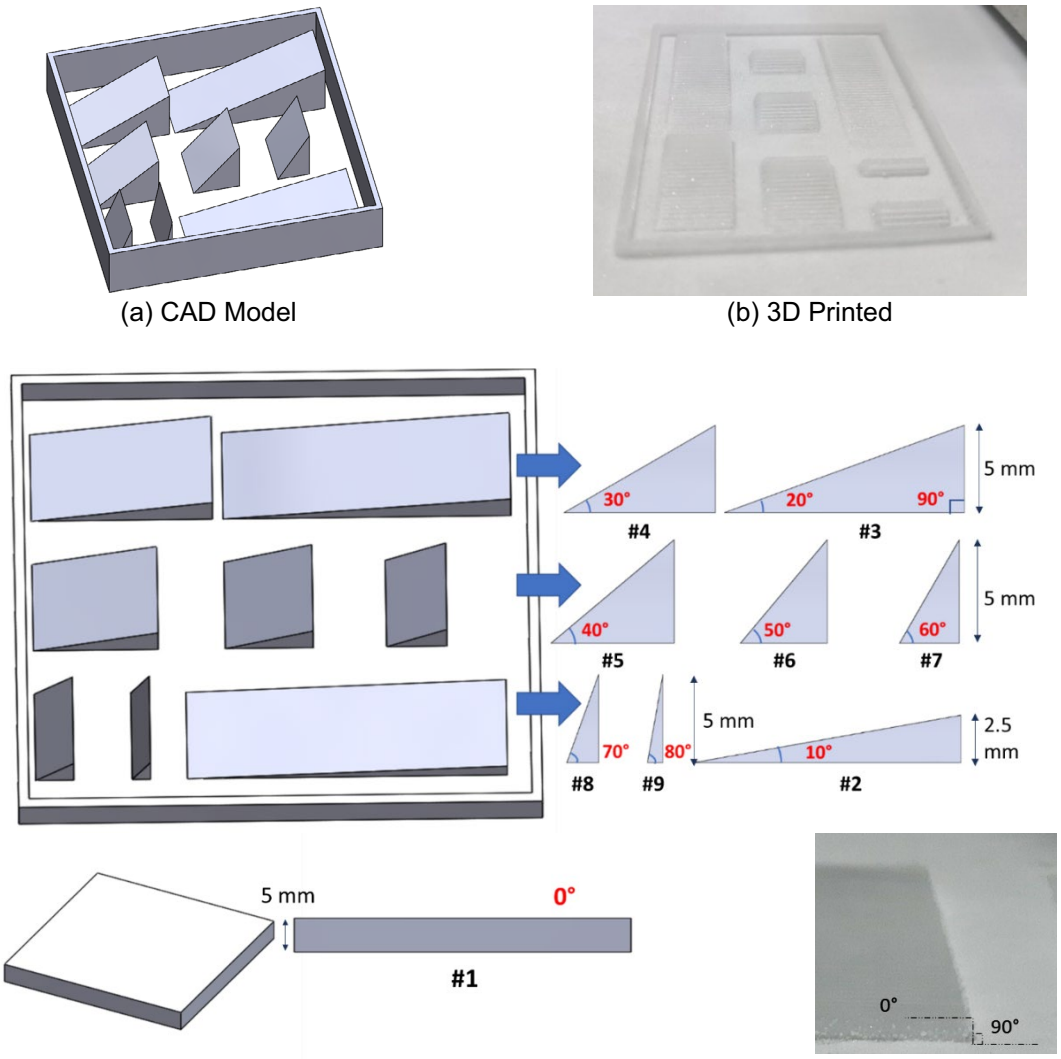

Fig. 10 Specimens for the test

3.1 Specimens

The specimen surfaces were 3D printed as shown in Fig. 10. The angles from 10° to 90° were printed as shown. A flat surface printed separately was used to measure the roughness of the horizontal surface (0°).

3.2 UV templating

It is difficult to measure the surface roughness of ice objects by traditional methods. Ice objects cannot be transported to the measuring instrument without causing geometry loss, and if left in the air for an extended period, ambient water vapour tends to condense on the surface. Therefore, surface finish is measured using an indirect, non-contact method termed as *templating* technique. The ice geometry to be measured is copied to another material with a significantly lower freezing point than ice and remains solid at ambient temperature.

UV resin, a liquid monomer with a solidification point of −8 °C, is helpful for this purpose. UV resin, pre-cooled to −2 °C, is poured as a thin layer on the ice object to be measured and allowed to settle for 15 s. A UV lamp with a wavelength of 400 nm is employed to cure the resin (Fig. 11a). Even at the sub-zero temperature of the build chamber, the resin polymerizes into a solid after 120 s. After curing, the lamp is removed, and the resin-covered ice object is removed. The ice object melts, leaving behind the desired geometry on the resin (Fig. 11b).

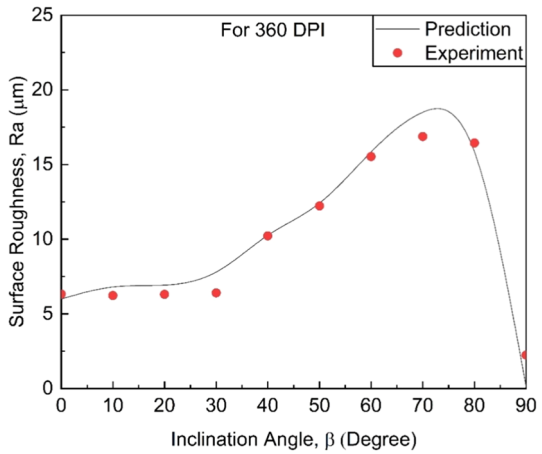

Fig. 12 Variation of surface roughness with surface inclination (360 DPI)

3.3 Measurement method

A 3D non-contact Surface Profilometer by Alicona (InfiniteFocus®) was used to measure the templates' surface roughness. The templates were neatly cut into the required sizes, the surface under observation was aligned horizontally by mounting properly. The mounted samples were neatly placed on the stage of the profilometer. A profile length of 1.4 mm was used. The values of Ra, Rq, Rt, Rz and Rmax were read from the interface of the IF-MeasureSuite software for Alicona. Measurements were carried out at the room temperature of 24 °C with 44% RH.

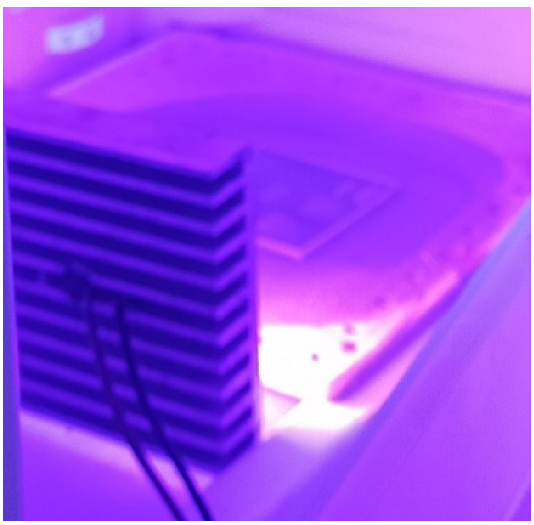

(a) Curing the resin covering the ice object

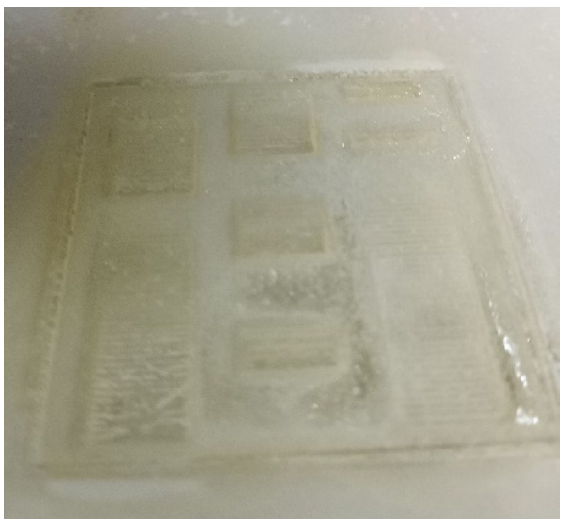

(b) Resin template having the geometry to be measured

Fig. 11 Investigation of surface roughness at various inclinations

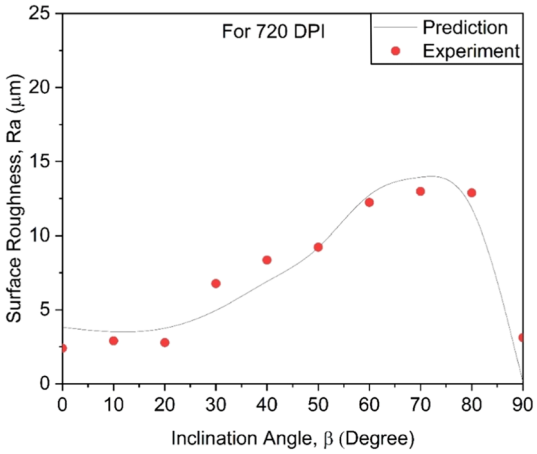

Fig. 13 Variation of surface roughness with surface inclination (720 DPI)

4 Results and discussion

In Figs. 12 and 13, the experimental results are displayed against the theoretical prediction. To comprehend the trend of surface roughness with surface orientation, the surface orientation is chosen for ten levels starting from 0° to 90° with an increment of 10°.

It is observed that the R_a value tends to increase with the increase in the inclination angle, a trend that is similar to the spherical cap model discussed by Krishan and Kumar. The experimental result matches the theoretical model's inclination range of 0–45°. From 45° to 60° inclination, the model predicts higher values of the R_a than what was experimentally found.

It could be because the model assumes the droplets are stacked above the other, and they all freeze at the same rate. Also, DPI is low, resulting in droplets being deposited sparser than those at 720 DPI (Fig. 13). It theoretically reduces the overlapped region between the adjacent droplets on the inclined surface, which predicts higher roughness values than expected. However, as the part height increases, the freezing time of the droplet also increases since the ice layers below the topmost layer act as insulators. It may allow more spread of the droplet resulting in more overlap.

The proposed model agrees well with the experiments at 720 DPI. Higher DPI results in closer droplets and higher overlap between the two beads, leading to a smoother surface than the 360 DPI case (Fig. 12). The average surface roughness is 20% lesser in 720 DPI case than in 360 DPI. It is observed that the proposed model agrees well with the experimental results at higher DPI values.

In the case of 90° inclination, the droplets are stacked vertically. As a result, DPI does not affect vertical surface roughness. The average surface roughness value found by the ice line model at 360 and 720 DPI is 0.1 μm. Although the empirically discovered R_a values are 20–30 times higher than the theoretically predicted value, they are closer to the R_a values predicted by Sui and Leu's ice line model (e.g., 5 μm roughly). Because the layers tend to expand out in reality, adding to the surface roughness, the experimental values are higher than predicted.

4.1 Comparison with the previous models

The proposed model combines the two existing models, viz., ice line and spherical cap model, that considers droplet sphericity and staircase effect. In the previous study by Krishnan and Gurunathan, the surface roughness ranges from 5 to 25 μm. Parts built with UV resin on polyjet in another study exhibit the surface roughness ranging from 0.2 to 23.82 μm depending on the print orientation [10]. It is observed by *the spherical cap model* that the surface roughness increases with an increase in the inclination angle, which agrees with the trend presented in this paper. ANOVA studies are also available, where the effect of the process parameters is discussed, where the type of finish has found to be the most influential parameter followed by surface orientation. Other parameters like layer thickness and the interactions between layer thickness and type of finish, layer thickness and local surface orientation were found less significant (<2%). Therefore, they are not considered for the present study. The present study is more focused on type of finish and surface orientation.

The proposed model agrees with the surface roughness values found by previous studies. The proposed model is developed and validated with a low contact angle of the ice-water interface ($12 \pm 1°$ at sub-zero temperatures); however, for the same contact angle range, the Krishnan–Gurunathan model predicts lower surface roughness values than experimentally found. It shows that the proposed model is more accurate since it considers the shape of the droplets.

4.2 Limitation of the proposed model

The proposed model is limited in predicting vertical surfaces' roughness. The proposed model fails to predict the roughness values of the vertical surfaces. Therefore, the ice line model is used for the vertical surface since it is free from any effects of the variation in the DPI. The roughness of the vertical surface is almost similar to the horizontal surface. The experiments are carried out for the multi-jet deposition at sub-zero temperatures. However, the model can be generalized for all material jetting processes.

5 Conclusion

In the droplet-based AM processes, droplet geometry as well as staircase effect play a vital role in determining the surface roughness. The presented model considers DPI and surface orientation. DPI indicates the proximity of the droplets, whereas part orientation indicates the staircase effect. Previous models, such as the ice line model, do not account for the inaccuracy caused by the staircase effect, and the spherical cap model does not account for bead geometry. The current model combines both approaches, considering the droplet (bead) shape and the staircase effect caused by an inclined surface.

The present model is useful in assessing the surface roughness of the parts based on the printing parameters. The parameters can therefore be adjusted to obtain the desired surface roughness range. The parts can be used as patterns for precision casting; for example, jewellery, dental and other biomedical implants, the surface roughness becomes an important aspect of the process. The desired surface roughness can be obtained on the casting as the precision casting offers net shape capability.

As future scope of this research, various liquids with different contact angles and the flow properties can be tested for their surface roughness to validate this model to make it more universally applicable.

Author contributions Study conception and experimental design: PK, mathematical model: YM, analysis and interpretation of the results: PK and GG, draft manuscript: SM, manuscript review and recommendation: KPK.

Funding This research did not receive any specific grant from funding agencies in the public, commercial, or not-for-profit sectors.

Data availability Experimental data will be shared upon a reasonable request.

Declarations

Conflict of interest The authors certify that they have No affiliations with or involvement in any organization or entity with any financial interest (such as honoraria; educational grants; participation in speakers' bureaus; membership, employment, consultancies, stock ownership, or other equity interest; and expert testimony or patent-licensing arrangements), or non-financial interest (such as personal or professional relationships, affiliations, knowledge or beliefs) in the subject matter or materials discussed in this manuscript.

Ethics The study does not include any human subjects, human data or tissue, or animals. Therefore, ethical clearance is not required.

References

1. Liu Q, Leu MC, Richards VL, Schmitt SM (2004) Dimensional accuracy and surface roughness of rapid freeze prototyping ice patterns and investment casting metal parts. Int J Adv Manuf Technol 24(7–8):485–495. https://doi.org/10.1007/s00170-003-1635-9
2. Sui G, Leu MC (2003) Investigation of layer thickness and surface roughness in rapid freeze prototyping. J Manuf Sci Eng 125(3):556. https://doi.org/10.1115/1.1556401
3. Liu Q, Sui G, Leu MC (2002) Experimental study on the ice pattern fabrication for the investment casting by rapid freeze prototyping (RFP). Comput Ind 48(3):181–197. https://doi.org/10.1016/S0166-3615(02)00042-8
4. Huang C, Leu MC, Richards VL (2004) Investment casting with ice patterns and comparison. NSF design manufacturing grantees conference, pp 1–7
5. Kamble P, Hodgir R, Gote G, Mittal Y, Karunakaran KP (2022) Sub-zero additive manufacturing: a review of peculiarities and applications of additive manufacturing at temperatures below 0°C. Prog Addit Manuf. https://doi.org/10.1007/s40964-022-00273-y
6. Bryant FD, Sui G, Leu MC (2003) A study on effects of process parameters in rapid freeze prototyping. Rapid Prototyp J 9(1):19–23. https://doi.org/10.1108/13552540310455610
7. Kechagias JD, Maropoulos S (2015) An investigation of sloped surface roughness of direct poly-jet 3D printing. Proc Int Conf Ind Eng, pp 150–153. Available http://www.inase.org/library/2015/zakynthos/bypaper/CIMC/CIMC-26.pdf.
8. Adel M, Abdelaal O, Gad A, Nasr AB, Khalil AM (2018) Polishing of fused deposition modeling products by hot air jet: evaluation of surface roughness. J Mater Process Technol 251(2017):73–82. https://doi.org/10.1016/j.jmatprotec.2017.07.019
9. Kumar K, Kumar GS (2015) An experimental and theoretical investigation of surface roughness of poly-jet printed parts: this paper explains how local surface orientation affects surface roughness in a poly-jet process. Virtual Phys Prototyp 10(1):23–34. https://doi.org/10.1080/17452759.2014.999218
10. Cazón A, Morer P, Matey L (2014) PolyJet technology for product prototyping: tensile strength and surface roughness properties. Proc Inst Mech Eng B J Eng Manuf 228(12):1664–1675. https://doi.org/10.1177/0954405413518515
11. Aslani KE, Vakouftsi F, Kechagias JD, Mastorakis NE (2019) Surface roughness optimization of poly-jet 3D printing using Grey Taguchi Method. Proc—2019 3rd Int Conf Control Artif Intell Robot Optim ICCAIRO 2019, pp 213–218. doi:https://doi.org/10.1109/ICCAIRO47923.2019.00041.
12. Vidakis N, Petousis M, Vaxevanidis N, Kechagias J (2020) Surface roughness investigation of poly-jet 3D printing. Mathematics 8(10):1–14. https://doi.org/10.3390/math8101758
13. Kechagias J, Iakovakis V, Giorgo E, Stavropoulos P, Koutsomichalis A, Vaxevanidis NM (2014) Surface roughness optimization of prototypes produced by polyjet direct 3D printing technology. OPT-i 2014 1st Int Conf Eng Appl Sci Optim Proc, vol 2014, pp 2877–2888
14. Udroiu R, Mihail LA (2009) Experimental determination of surface roughness of parts obtained by rapid prototyping. Proc 8th WSEAS Int Conf Circuits, Syst Electron Control Signal Process, January 2015, pp 283–286. Available: http://www.wseas.us/e-library/conferences/2009/tenerife/CSECS/CSECS-50.pdf
15. Cheng YL, Chang CH, Kuo C (2020) Experimental study on leveling mechanism for material-jetting-type color 3D printing. Rapid Prototyp J 26(1):11–20. https://doi.org/10.1108/RPJ-09-2018-0227
16. Collins W, Hass A, Jeffery K, Martin A, Medeiros R, Tomljanovic S (2015) Graphic design and print production fundamentals. Graphic Communications Open Textbook Collective licensed under Creative Commons Attribution 4.0 International License. Victoria, B.C.: BCcampus. Retrieved from https://opentextbc.ca/graphicdesign/
17. Li S, Liu M, Hanaor D, Gan Y (2018) Dynamics of viscous entrapped saturated zones in partially wetted porous media. Transp Porous Media 125(2):193–210. https://doi.org/10.1007/s11242-018-1113-3

18. Suryakumar S, Karunakaran KP, Bernard A, Chandrasekhar U, Raghavender N, Sharma D (2011) Weld bead modeling and process optimization in hybrid layered manufacturing. CAD Comput Aided Des 43(4):331–344. https://doi.org/10.1016/j.cad.2011.01.006
19. Gonzalez-Gutierrez J, Cano S, Schuschnigg S, Kukla C, Sapkota J, Holzer C (2018) Additive manufacturing of metallic and ceramic components by the material extrusion of highly-filled polymers: a review and future perspectives. Materials (Basel) 11(5):840. https://doi.org/10.3390/ma11050840
20. Bourell D et al (2017) Materials for additive manufacturing. CIRP Ann Manuf Technol 66(2):659–681. https://doi.org/10.1016/j.cirp.2017.05.009
21. Zhang W, Leu MC, Ji Z, Yan Y (1999) Rapid freezing prototyping with water. Mater Des 20(2–3):139–145. https://doi.org/10.1016/S0261-3069(99)00020-5
22. Sijpkes P, Barnett E, Angeles J, Pasini D (2009) The architecture of phase change at McGill. Leadersh Archit Res, p 241
23. Zhang HZ et al (2015) Portable, easy-to-operate, and antifouling microcapsule array chips fabricated by 3D ice printing for visual target detection. Anal Chem 87(12):6397–6402. https://doi.org/10.1021/acs.analchem.5b01440
24. Zheng F, Wang Z, Huang J, Li Z (2020) Inkjet printing-based fabrication of microscale 3D ice structures. Microsyst Nanoeng 6(1):89. https://doi.org/10.1038/s41378-020-00199-x
25. Kamble PP, Chavan S, Hodgir R, Gote G, Karunakaran KP (2021) Multi-jet ice 3D printing. Rapid Prototyp J 28(6):989–1004. https://doi.org/10.1108/RPJ-03-2021-0065